Chalcogenide Letters Vol. 17, No. 5, May 2020, p. 229 - 241

RESISTIVITY-TEMPERATURE DEPENDENCE, THERMAL AND ELECTRICAL PARAMETERS OF $Se_{65-x}As_{35}Sb_x$ THIN FILMS: (1µm, 5 K.min^{-1})

A. GADALLA[a], E. R. SHAABAN[b,*], F. A. ANAS[a], S. RAFIQUE[c], E. S.YOUSEF[d,e]

[a]*Physics Department, Faculty of Science, Assiut University, Assiut, Egypt*
[b]*Physics Department, Faculty of Science, A1-Azhar University, Assiut 71542, Egypt*
[c]*Multidisciplinary Nanotechnology Centre, College of Engineering, Swansea University, Swansea SA1 8EN, United Kingdom*
[d]*Physics Department, Faculty of Science, King Khalid University, P.O. Box 9004, Abha, Saudi Arabia*
[e]*Research Center for Advanced Materials Science (RCAMS), King Khalid University, Abha 61413, P.O. Box 9004, Saudi Arabia*

Sheet resistance, R_s, measurements for the ($Se_{65-x}As_{35}Sb_x$ thin films with ($0 \le x \ge 10$) at. %) with thickness film 1000 nm and heating rate, 5 K/min has been explained in this work. Measurements of the sheet resistance used to compute the thermal and electrical parameters in the temperature range from 300 to 665 K. In the sheet resistance curves, two main regions have been considered clearly evidence of one crystallization region for the studied films. The activation energy, E_c, of crystallization and Avrami index, n, were estimated. The change of activation energy with volume of crystalline fraction has been deduced. The electrical results of the studied films appear two types of conduction channels which contribute two conduction mechanisms in crystallized region. The activation energies ΔE, two pre-exponential factors σ_0, σ_0^* and other parameters has been computed in both of the extended and hopping states regions. The crystalline phases for the as-deposited and annealed films were identified using by x-ray diffraction (XRD).

(Received January 18, 2020; Accepted May 5, 2020)

Keywords: Sheet resistance, $Se_{65-x}As_{35}Sb_x$ thin films, The thermal and electrical properties, Crystallization parameters

1. Introduction

Chalcogenide glasses contain one or more chalcogen element (Se, S, Te) which produces covalent bonds with the network formers like As, Sb, Ge, etc. Because of the high atomic masses and hence the low phonon energies in these elements, the transmission range extends into infrared region making it a suitable candidate for many applications in medical imaging, telecommunication, bio-sensing, infrared waveguides, optical fibers [1-4]. These materials appear a continuous alteration in many physical properties with alteration in chemical composition [5]. Many investigations of the electrical properties [6, 7], photo-conductivity [8], glass formation [9], study of structure [10] and analysis of crystallization kinetics [11-13] of the glassy (As–Se–Sb) system have been made. To our knowledge, less detailed investigations have been performed on their optical properties. In addition, more efforts have been carried out to develop the mathematical formulation describing both the reflectance and the transmittance of different optical systems.

* Corresponding author: esam_ramadan2008@yahoo.com

In such framework, the resistivity-temperature dependence of the $Se_{65-x}As_{35}Sb_x$ thin films with ($0 \leq x \geq 10$) at. %) are studied. Thus, we can calculate the thermal and electrical parameters for the studied films based on their surface resistance as a function of temperature. The crystallized phases were verified over the temperature that applied to the thin films by the technology of XRD.

2. Experimental details

Bulk chalcogenide of ($Se_{65-x}As_{35}Sb_x$ with ($0 \leq x \geq 10$) at. %) were prepared by the usual melt quench technique. Highly pure materials (with 99.999%) were weighted according to their atomic percentages, by an electrical balance type (Sartorius) with accuracy ($\pm 10^{-4}$ g) and sealed in evacuated silica tube (10^{-3} Pa) and it was heated at 1000 ^{o}C with the temperature ramp about 5 °C/min for 24 hours. During the melting process, the ampoule was inverted at regular time intervals (~ 1 h) so that the amorphous solid will be homogenous and isotropic. After the synthesis, the melt was quenched rapidly in ice water to obtain the $Se_{65-x}As_{35}Sb_x$ glassy alloy. Then the solid was broken along its natural stress line into smaller pieces suitable for grinding. The different compositions of $Se_{65-x}As_{35}Sb_x$ with ($0 \leq x \geq 10$ at. %) thin films were prepared by evaporating the powdered chalcogenide samples from a resistance heating quartz glass crucible onto dried precleaned glass substrates kept at room temperature, using a conventional coating unit (Denton Vacuum DV 502 A). The films were deposited onto glass substrates at a pressure of about $1x10^{-6}$ Pa.

Both the film thickness and the deposition rate (was about 20 Å/s) were monitored using FTM6 thickness monitor. The elemental composition of the films was analyzed using energy dispersive X-ray spectrometer (EDX) interfaced with a scanning electron microscope, SEM (JOEL XL) operating an accelerating voltage of 30 kV. The relative error of determining the indicated elements does not exceed 2%. X-ray powder diffraction (XRD) Philips diffractometry (1710), with Cu-Kα1 radiation (λ = 1.54056 Å) has been used to examine the structure of the as-prepared thin films. The data collection was performed by step scan mode, in a 2θ range between 5° and 80° with step-size of 0.02° and step time of 0.6 s.

3. Results and discussion

3.1. Resistivity-Temperature dependence, R_s-T

Fig. 1 plots the relationship between sheet resistance, R_s and temperature of chalcogine ($Se_{65-x}As_{35}Sb_x$ with ($0 \leq x \geq 10$) at. %) thin films (1000 nm), at heating rate 5 K/min**.** The R_s curves decrease continuously until an abrupt drop appears at 444.918, 449.137, 452.104, 458.038 and 461.179 K for corresponding studied films, respectively, and these temperatures called the crystallization temperatures, T_c, this gradient continues until it gets to the highest degree of crystallization, T_p and then the resistivity decreases in a continuous behavior after that. The R_s curves decrease gradually but slowly in the range of temperature (300-465K). In this range, the state of the studied films is amorphous and the arrangement of atoms is random, causing its high R_s values. The temperature is increased above T_c, the atoms have sufficient energy to rearrange. The transform of films from amorphous to crystalline state is due the arrangement of atoms and thus the *Rs* rapidly decrease. The decrease of *Rs* values is due to the grain growth of the films proceeding when the temperature is increased [14]. The noticed values for T_c and T_p are presented in Table 1.

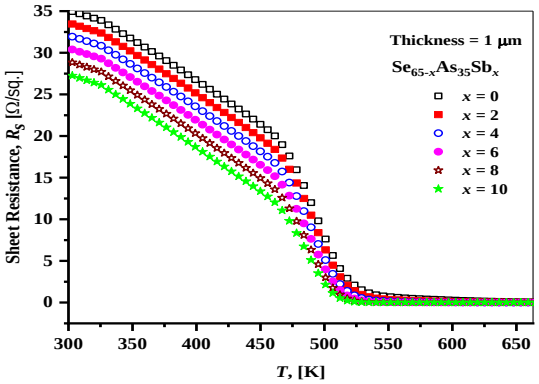

Fig. 1. Relationship between resistivity, (R_s) and temperature, T, for the ($Se_{65-x}As_{35}Sb_x$ with ($0 \le x \ge 10$) at. %) thin films.

Table 1. Maximum crystallization rate $(\frac{d\chi}{dt})$, temperature of crystallization (T_c), top crystallization temperatures (T_p), kinetic exponent, n and crystallization activation energy, E_C, according to method of for the ($Se_{65-x}As_{35}Sb_x$ with ($0 \le x \ge 10$) at. %) thin films.

$x\,[at.\%]$	$(\frac{d\chi}{dt})_p \times 10^3 (\min^{-1})$	T_C	T_p	n	$\langle n \rangle$	$E_C[KJ/mole]$	$E_C[eV]$
0	2.46083	457.523	492.166	3.29636	3.21	69.66	16.66
2	2.44645	455.638	489.291	3.23893		70.33	16.82
4	2.44199	453.754	488.397	3.22121		70.76	16.93
6	2.43589	451.869	487.178	3.19715		72.89	17.43
8	2.4298	449.985	485.96	3.17323		74.52	17.82
10	2.42704	448.101	485.408	3.16242		76.34	18.26

Then, the derivation of resistivity, R_s from the first degree relative to the temperature will lead us to know the first pillar of thermal investigations. Fig. 2 represents the relationship between the derivative of sheet resistance, $[dR_s/dT]$ and temperature, T. Now, the exothermic heat flow is given by the subsequence equation:

$$\Delta Q_{exo} = -[\frac{dR_s}{dT}]_{endo.} \quad (1)$$

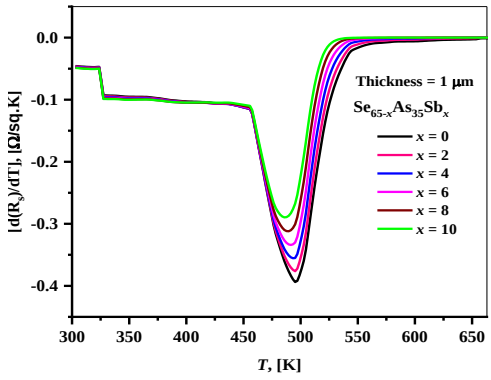

Fig. 2. Relationship between derivative of sheet resistance, dR_s/dT and temperature, T, for the ($Se_{65-x}As_{35}Sb_x$ with ($0 \le x \ge 10$) at. %) thin films.

Fig. 3 plots the exothermic heat flow, ΔQ_{exo} against temperature, T based on Eq. (1), for the first film. In the mentioned figure, χ_T, represents the crystallized fraction at a given temperature which expressed by relationship, $\chi_T = A_T / A$, where A is the total area of the peak and A_T is the area of crystallized part (the area between T_i and a given temperature, T). Both T_i and T_f are the initial and final crystallization temperature, respectively.

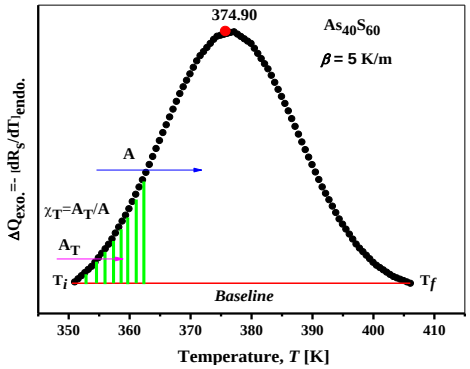

Fig. 3. The exothermic heat flow and the fraction, χ, crystallized at a given temperature, T, for the ($Se_{65-x}As_{35}Sb_x$ with ($0 \leq x \geq 10$) at. %) thin films.

The same way, the area under the crystallization peak is directly proportional to the total amount of alloy crystallized. The ratio between the selected ordinates and the total area of the exothermic peak represents the corresponding crystallization rates, which make it possible to plot the curves between volume crystallization fraction and temperature. The graphical of the volume fraction crystallized, (χ) shows the typical sigmoid curve as a function of temperature at heating rate (5 K/min) for studies films as shown in Fig. 4 and expressed by:

$$\chi = \sum_{i=0}^{s} \Delta Q_{exo} \; / \sum_{i=0}^{99} \Delta Q_{exo} \qquad (2)$$

where, s is number of points of the exothermic heat flow, ΔQ_{exo}, (namely, s=0 to 99).

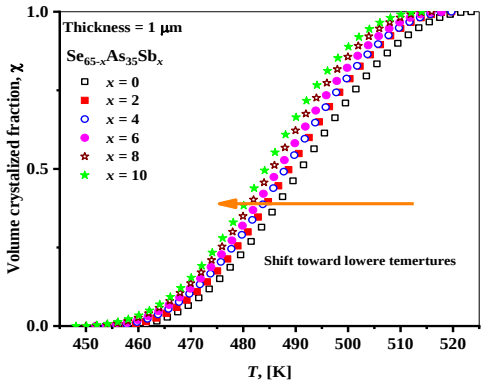

Fig. 4. Maximum crystallization rate, $(^{d\chi}/_{dt})_p$ versus temperature, T, of the exothermal peaks for the ($Se_{65-x}As_{35}Sb_x$ with ($0 \leq x \geq 10$) at. %) thin films.

Now**,** the relationship between crystallization rate, $(d\chi/dt)$ and the temperature produced by differentiating of the volume crystallized fraction as a function of time, which expressed by the subsequent equation for the maximum crystallization rate:

$$(\frac{d\chi}{dt})_p = \frac{dT}{dt} \times (\frac{d\chi}{dT})_p = \beta \times (\frac{d\chi}{dT})_p = \beta \times T_p \tag{3}$$

here, β is the heating rate.

Fig. 5 represents the crystallization rate $(d\chi/dt)$ as a function of temperature. The values of the maximum crystallization rate computed based on Eq. (3) and listed in Table 1. From Fig. 4 and Fig. 5, one can infer that the saturation of crystallization shifts towards the lower temperature when the Sb content for the investigated films increases.

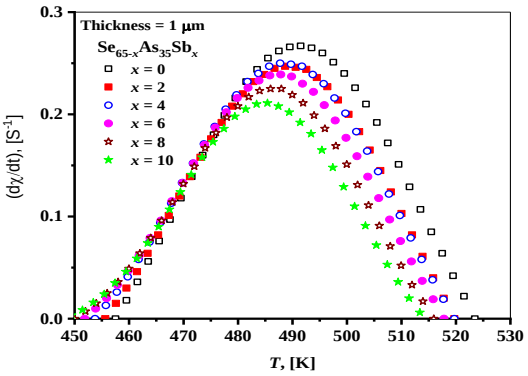

Fig. 5. The typical sigmoid curve of the volume fraction crystallized, χ, as a function of temperature, T, for the ($Se_{65-x}As_{35}Sb_x$ with ($0 \leq x \geq 10$) at. %) thin films.

3.2. Determination of the activation energy

In this framework, we will address the methods of Kissinger and Matusita to determine the activation energy for the investigated films.

3.2.1. Method of Kissinger

Kissinger method relies on the determination of the peak temperature, T_p from experiments carried at different heating rates β [15]. According to this approach, the activation energy, E_c of amorphous-crystalline transformation was originally computed via the subsequence relationship [15] as:

$$\ln\left(\beta/T_p^{\,2}\right) = E_c/RT_p - \ln(E_c/RK_0) \tag{4}$$

According to Kissinger's approach, the maximum reaction rate occurs at peak temperature, T_p. A plot of $\ln\left(\beta/T_p^{\,2}\right)$ against $(1000/T_p)$ gives the values of the pre-exponential factor, K_0 and the activation energy, E_c. Fig. 6 draws $\ln\left(\beta/T_p^{\,2}\right)$ against $(1000/T_p)$ for the studied films. The activation energy, E_c and frequency factor, K_0, are determined by least squares fitting method. The values for both E_c and K_0 equal to 8.1266 eV, 3.45×10^7, respectively.

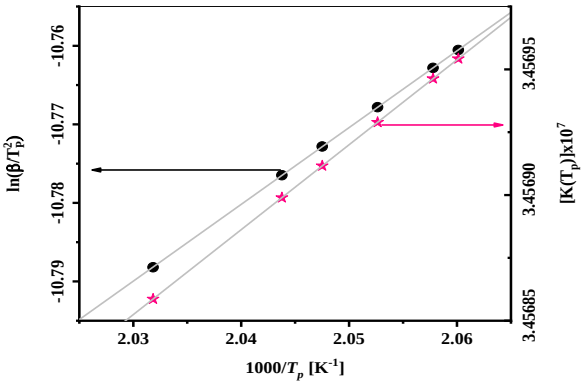

Fig. 6. The plot of $\ln(T_p^2/\beta)$ *and* $K(T_p)$ *as a function of* T_p *versus* $(1000/T_p)$ *for the* $(Se_{65-x}As_{35}Sb_x$ *with* $(0 \le x \ge 10)$ *at. %) thin films.*

By a similar perspective, the temperature-dependent rate constant □(□) follows the Arrhenius type in the equation:

$$K(T) = K_0 \exp[-\frac{E_c}{RT}] \tag{5}$$

where, *R* is the universal gas constant and equals to 8.314 KJ/mole. In addition, a kinetic parameter, *K (T)*, with Arrhenian temperature dependence, is submitted to the stability criteria. According to Surinach *et al*. [16] and Hu and Jiang [17] the thermal stability of glassy materials estimates by the following criterion as:

$$K(T_p) = K_0 \exp[-\frac{E_c}{RT_p}] \tag{6}$$

The value of this criterion allusive the tendency of glass to devitrify on heating, whereas the glass formation is a kinetic process. $K(T_p)$, as a function of, T_p, for the studied samples is shown in Fig. 7.

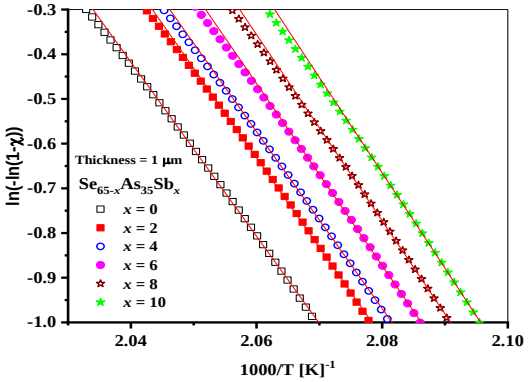

Fig. 7. The plot of $\ln(-\ln(1-\chi))$ *versus* $1000/T$ *for the* $(Se_{65-x}As_{35}Sb_x$ *with* $(0 \le x \ge 10)$ *at. %) thin films.*

Furthermore, from the experimental values of $(d\chi/dt)_p$, we can determine the kinetic exponent, *n* by the subsequence equation:

$$n = \frac{RT_p^2 \times (d\chi/dt)_p}{0.37\beta E_c} \tag{7}$$

The *n* values for investigated samples are computed and tabulated in Table 1. Finally, the experimental data, T_p , and $(d\chi/dt)_p$, are shown also in Table 1 and the values of the activation energy of crystallization process for the crystallization peaks which get from Kissinger method in crystallization region (8.1266 eV), make it possible to computed, through Eq. (6), the kinetic exponent, *n*, for the experimental heating rate (5 K/min) for the peaks of investigated samples, whose values are also tabulated in Table 1. The kinetic exponent, *n* was computed based on the mechanism of crystallization Mahadevan *et al.* [18] have appeared that *n* may be 4, 3, 2, which are related to different glass-crystal transformation mechanisms: *n* = 4, volume nucleation, three-dimensional growth; *n* =3, volume nucleation, two-dimensional growth, *n* = 2, volume nucleation, one-dimensional growth; *n* = 1, surface nucleation, one-dimensional growth from surface to the inside. Therefore, bearing in mind the above obtained mean values for crystallization region (as shown in Table 1) means volume nucleation, one-dimensional growth because values is integer, namely, *m*=*n*-1=1. The computed *n* values are not integers. This means that the crystallization occurs by more than one mechanism [19, 20].

3.2.2. Method of Matusita

The Matusita model evidences the importance of the factor *m* for the determination of the activation energy of the crystallization process. This fact is related to the nucleation and growth of the crystallites in the amorphous matrix. Furthermore, the activation energy E_c of the investigated samples was computed using bythe Matustia relationship [21]:

$$\ln(-\ln(1-\chi) = -n\ln\beta - 1.052\frac{mE_c}{RT} + const. \tag{8}$$

where (*m*=*n*-1) is the dimension order parameter and (*n*) is constant related to the crystallization mechanism as mentioned above. Plots $\ln(-\ln(1-\chi)$ versus $1000/T$ for the investigated samples (at heating rate equal to 5 K/min) are shown in Fig. 8. For the computation of E_c we take into consideration the linear region of this plot. From the average, *n* values and mE_c (*n*=*m*+1), the effective activation energies E_c for the studied samples is computed and listed in Table 1. Now, if we examine the two models, namely, Kissinger's model and Matusita model, the Kissinger model is opposite to the model of Matusita, it is considered that on the top of crystallization peak the amount of crystallized fraction.

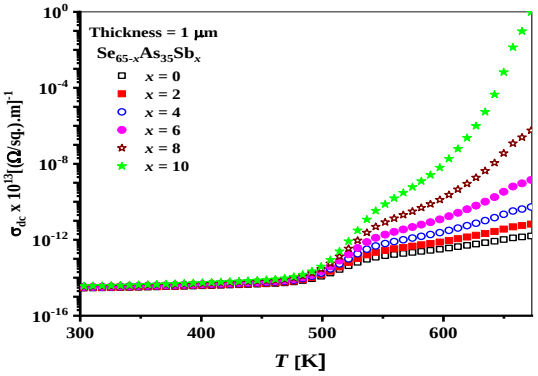

Fig. 8. The dark electrical conductivity, σ (T) as a function of temperature, T for the ($Se_{65-x}As_{35}Sb_x$ with ($0 \leq x \geq 10$) at. %) thin films.

4. Electrical conductivity-Temperature dependence

Post-prepared Al electrodes in a square geometry (5.0 mm) were used for resistance-temperature measurements, carried out in the running vacuum. It was reported that sheet resistance (R_s, Ω/sq.), independent of the investigated samples area, was helpful instead of resistivity, ρ in order to examine the electrical properties of the films [22], and then the resistivity, ρ can be extracted from the following relationship:

$$\rho_{dc}(T) = R_s \times d \tag{9}$$

where d is thickness of the investigated films and it equals to 1000 nm. On the other hand, the dark electrical conductivity, σ (T) is given by the following equation:

$$\sigma_{dc}(T) = [1/\rho_{dc}(T)] = [1/(R_s \times d)] \tag{10}$$

Now, the effect of heat treatment on the electrical conductivity, σ (T) of the as-deposited thin films, with ($0 \leq x \geq 10$ at. %,), thickness, 1000 nm deposited onto glass substrate held at room temperature was studied. The computations were taken in the ranging from 300 up to 665 K. The dark electrical conductivity σ (T) as a function of temperature for the investigated films is presented in Fig. 9. We clearly observe from Fig. 9 that conductivity increases with increasing both temperature and selenium content in the studied system. On the other hand, the dark electrical conductivity σ (T) as a function of reciprocal temperature for the studied films is shown in Fig. 10. From Fig. 10, we notice that the electrical results exhibit two types of conduction channel which contribute two conduction mechanisms. In the range of temperature (465-665K), the electrical conductivity shows a slight increase with increasing temperature and corresponds to transport by hopping conduction, while the increasing is rapidly in range of temperature (300-465 K) where the energy states are extended between the valence and conduction band. The values of activation energy (ΔE) and pre-exponential factor σ_0 in every range were computed and listed in Table 2. The two parameters changed with temperature in an exactly opposite behavior in the extended states region and in the same behavior in the hopping states region and these results correspond to similar results in search [23, 24]. This confirms that the change in σ is connected to a corresponding change in ΔE.

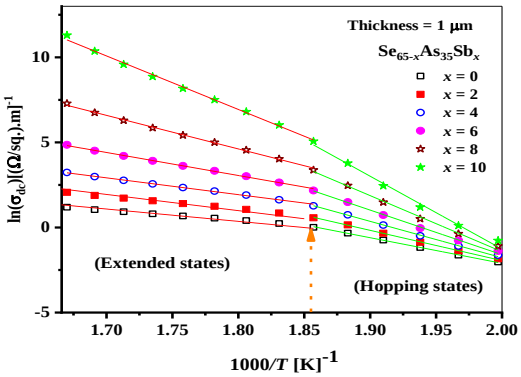

Fig. 9. The logarithm dark electrical conductivity, ln[σ (T)] as a function of reciprocal temperature, (1000/T) for the ($Se_{65-x}As_{35}Sb_x$ with ($0 \le x \ge 10$) at. %) thin films.

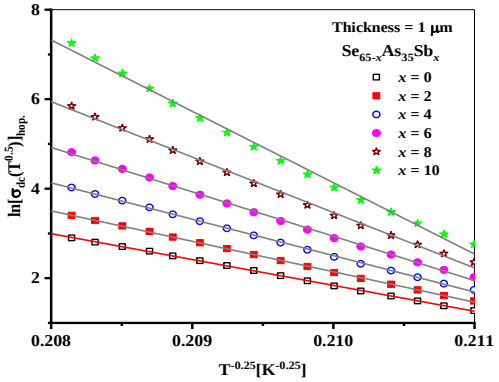

Fig. 10. The linear plots of $\ln[\sigma_{hop.}.\sqrt{T}\,]$ *versus* $[1/\sqrt[4]{T}\,]$ *for the ($Se_{65-x}As_{35}Sb_x$ with ($0 \le x \ge 10$) at. %) thin films.*

Table 2. The values of activation energy, (ΔE) by unit [eV] and pre-exponential factor σ_0 *by unit [* $(\Omega cm)^{-1}$ *] in every studied range of temperature, where (ext.) refers to extended states and (hop.) refers to hopping states for the ($Se_{65-x}As_{35}Sb_x$ with ($0 \le x \ge 10$) at. %) thin films.*

Hopping states region		**Extended states region**		$x\,[at.\%]$
$\Delta E_{Hop.}$ **[eV]**	$\ln(\sigma)_{Hop.}$ $(\Omega cm)^{-1}$	$\Delta E_{ext.}$ **[eV]**	$\ln(\sigma)_{ext.}$ $(\Omega cm)^{-1}$	
1.29781	27.9881	0.62587	13.42061	**0**
1.53456	33.63643	0.82118	18.12741	**2**
1.84415	40.98505	0.8514	19.69834	**4**
2.26071	50.82236	1.1677	27.42376	**6**
2.8417	64.47182	1.70142	40.12423	**8**
3.69082	84.31651	2.71279	63.55134	**10**

New, the measured conductivity is the sum of two components to compute the density of states at the Fermi level, N (E_F):

$$\sigma_{dc}(T) = \sigma_{hop.} + \sigma_{ext.} \tag{11}$$

Here, $\sigma_{hop.}$ is the contribution of conduction due to hopping between the nearest localized states and $\sigma_{ext.}$ is the contribution of conduction between the extended states show activated temperature dependence based on the relation:

$$\sigma_{ext.} = \sigma_0 \times \exp[-\frac{\Delta E_0}{K_B T}] \tag{12}$$

where ΔE_0 and σ_0 are the activation energy and pre-exponential factor, respectively. In range of temperature (465-665 K), the contribution occurs by variable range hopping of the charge carriers in the localized states near the Fermi level, and is characterized by Mott's variable-range hopping relation [25]:

$$\sigma_{hop.} = \frac{1}{\sqrt{T}}[\sigma_0^* \times \exp[-\frac{A}{\sqrt[4]{T}}] \tag{13}$$

And

$$A^4 = T_0 = \frac{\gamma \times \alpha^3}{K_B \times N(E_F)} \tag{14}$$

where $N(E_F)$ is the density of localized states at the Fermi level, α is the coefficient of exponential decay of the localized state wave function and it is assumed to be 1.24*10 ^{7}cm^{-1} [26] and K_B is Boltzmann's constant, T_0 the degree of disorder and it has temperature dimensions and γ is the Debye frequency≈ (10^{13} Hz). The value of σ_0^* obtained by various workers [30, 31]:

$$\sigma_0^* = (3e^2\gamma) \times \sqrt{\frac{N(E_F)}{8\pi\alpha K_B T}} \tag{15}$$

Here, e is the electron charge. The density of states at the Fermi levels $N(E_F)$ has been calculated for this sample and listed in Table 3.

Table 3. Mott's parameters in hopping range of temperature (465- 665 K) for the ($Se_{65-x}As_{35}Sb_x$ with ($0 \le x \ge 10$) at. %) thin films.

At T= 400 K		$N \times 10^{14}$	$N(E_F) \times 10^{15}$	$T_0 \times 10^{11}$	$\sigma_0^* \times 10^{-14}$	x [at.%]
ψ_h [eV]	$R_h \times 10^{-6}$ [cm]	[cm^{-3}]	[$eV^{-1}cm^{-3}$]	[K]	[$(\Omega cm)^{-1}.(K)^{-0.5}$]	
0.898	4.203	2.468	3.576	1.112	0.664	**0**
1.058	4.950	1.283	1.860	2.138	0.345	**2**
1.266	5.921	0.626	0.908	4.380	0.168	**4**
1.543	7.221	0.283	0.410	9.684	7.629	**6**
1.927	9.016	0.116	0.169	23.543	3.138	**8**
2.481	10.160	0.042	0.061	64.630	1.143	**10**

When stated by Mott [25] and Hill [29] three other hopping parameters can be computed, hopping distance R (cm), the average hopping energy ψ_h (eV) and the concentration of conduction electrons N, these parameters are given by [27]:

$$R = [\frac{9}{8\pi K_B T . N(E_F)}]^{0.25} \tag{16}$$

$$\psi_h = \frac{1}{4} K_B T^{3/4} T_0^{1/4} \tag{17}$$

$$N = 2K_B T . N(E_F) \tag{18}$$

The determined values of R, ψ_h and N (at T= 400 K) for the samples under investigation are also tabulated in Table 3. The linear plots of, $\ln[\sigma_{hop.}\sqrt{T}]$, versus $1/\sqrt[4]{T}$ for the investigated thin films is presented in Fig. 11. Mott's parameters for the studied thin films computed and listed in Table 3. It is observed for the studied films that values of R and W decrease while N increases with increasing Se content. Also, the computed parameters, $W > k_BT$, $\alpha R > 1$ and $T_o > 10^3$ K, agree well with the requirement for the validity of VRH model [27-30].

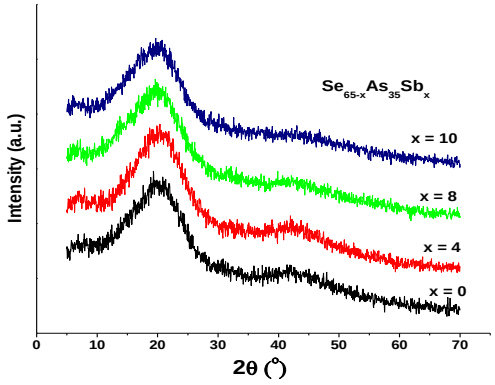

Fig. 11. X-ray diffraction pattern of as-prepared for the ($Se_{65-x}As_{35}Sb_x$ with $(0 \leq x \geq 10)$ at. %) thin films.

5. Identification of the crystalline phases

The nature of transformation from amorphous to crystalline state of the studied as-deposited thin films was confirmed by (XRD) measurements as shown in Fig. 11. The absence of any peak in the XRD scan of the as-deposited films confirms their amorphous nature. But, the diffract gram of an annealed films at 460 K appears sharp peaks as shown in Fig. 11. The sharp peaks indicate the development of amorphous structure along with ploy-crystalline phases during the thermal heat treatment of investigated films. The diffraction of dominant peaks were indexed with Sb_2Se_3 phase [No. card: 15-861] and As_2Se_3 phase [No. card: 26-123] for an annealed films at 460 K) along their respective 2Θ value (JCPDS database, 1998) as shown in Fig. 12.

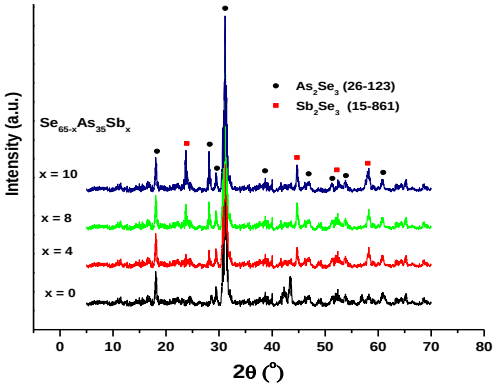

Fig. 12. X-ray diffraction pattern of annealed $Se_{65-x}As_{35}Sb_x$ thin films at 640 K

6. Conclusions

($Se_{65-x}As_{35}Sb_x$ thin films, with ($0 \leq x \geq 10$) at. %) were successfully synthesized using by a homogeneous precipitation method. The studied films were deposited by thermal evaporation technique. The experimental structural, thermal and electrical properties of thermally evaporated thin films (1000 nm) of the studied thin films at heating rate equals to 5 K/min, have been discussed based on sheet resistance, R_s measurements. The R_s decreases continuously in the range from 300 under to 465 K, until an abrupt drop shows at the temperatures that called the crystallization temperatures, (T_c), this gradient continues until it gets to the highest degree of crystallization, T_p and then the sheet resistance decreases in a continuous behavior in the range (465-665K). Then, the thermal properties and kinetics parameters such the activation energy of amorphous-crystalline transformation E_c, the Avrami exponent *n*, the frequency factor, K_0, have been determined. Finally, the temperature-dependent sheet resistance, R_s measurements of the as-deposited films at heating rate (5 K/min), was investigated and from it we have been detected several of electrical parameters. One of the most important of these parameters is the activation energy that has the same behavior of pre-exponential factor in both regions.

Acknowledgments

The authors are grateful to Assiut University and Al-Azhar University for supporting this work. In addition, the authors thank the Deanship of Scientific Research at King Khalid University (KKU) for funding this research project, Number: (R.G.P2./62/40) under research center for advanced material science.

References

[1] J. Solis et al., Physical review letters **76**(14), 2519 (1996).
[2] J. H. Coombs et al., Journal of applied physics **78**(8), 4906 (1995).
[3] E. R. Shaaban, M. S. Abd El-Sadek, M. El-Hagary, I. S. M. Yahia, Physica Scripta **86**(1), 015702 (2012).
[4] R. Frerichs, Physical Review **78**(5), 643 (1950).
[5] ELS Yousef, A. El-Adawy, N. El Koshkhany, E. R. Shaaban, Journal of Physics and Chemistry of Solids **67**(8), 1649 (2006)
[6] Pramod K. Khulbe et al., Applied optics **41**(29), 6220 (2002).
[7] B. J. Kooi, J. Th. M. De Hosson, Journal of applied physics **95**(9), 4714 (2004).
[8] A. Goel, E.R. Shaaban. D.U. Tulyaganov, J.M.F. Ferreira, Journal of the American Ceramic Society **91**(8), 2690 (2008).
[9] L. Van Pieterson et al., Journal of Applied Physics **97**(8), 083520 (2005).
[10] Huai-Yu Cheng et al., IEEE transactions on magnetics **43**(2), 927 (2007).
[11] Tong Ju et al., Journal of Non-Crystalline Solids **354**(19-25), 2662 (2008).
[12] Homer E. Kissinger, Analytical chemistry **29**(11), 1702 (1957).
[13] S. Surinach et al., Journal of materials science **19**(9), 3005 (1984).
[14] E.R . Shaaban, M.A Kaid,. M.G.S. Ali, Journal of Alloys and Compounds 613, 324 (2014).
[15] Homer E. Kissinger, Analytical chemistry **29**(11), 1702 (1957).
[16] S. Surinach et al., Journal of materials science **19**(9), 3005 (1984).
[17] L. Hu, Z. Jiang, J. Chin, Ceram Soc. **18,** 315 (1990).
[18] Sudha Mahadevan, A. Giridhar, A. K. Singh, Journal of Non-Crystalline Solids **88**(1), 11 (1986).
[19] P. Duhaj, D. Barančok, A. Ondrejka, Journal of Non-Crystalline Solids **21**(3), 411 (1976).
[20] Keiji Tanaka, Physical Review *B* **39**(2), 1270 (1989).
[21] Kazumasa Matusita, Takayuki Komatsu, Ryosuke Yokota, Journal of Materials Science

19(1), 291 (1984).
[22] Walter K.Njoroge, Han-Willem Wöltgens, Matthias Wuttig, Journal of Vacuum Science & Technology A: Vacuum, Surfaces, and Films **20**(1), 230 (2002).
[23] Martin Wimmer et al., Frontiers in Physics **2**, 75 (2014).
[24] M. I. Abd-Elrahman et al., Applied Physics A **122**(8), 772 (2016).
[25] N. F. Mott, E. A. Davis, R. A. Street, Philosophical Magazine **32**(5), 961 (1975).
[26] S. Chaudhuri et al., Journal of Non-Crystalline Solids **46**(2), 171 (1981).
[27] E. A. Davis, N. F. Mott, Philosophical Magazine **22**(179), 0903 (1970).
[28] A. Touraine, C. Vautier, D. Carles, Thin Solid Films **9**(2), 229 (1972).
[29] Robert M.Hill, Philosophical Magazine **24**(192), 1307 (1971).
[30] Nevill Francis Mott, Edward A. Davis, *Electronic processes in non-crystalline materials*, OUP Oxford, 2012.